On the theory of layered high-temperature superconductors

Schneider, T.; Raedt, H. De; Frick, M.

Published in:
Zeitschrift für Physik. B: Condensed Matter

DOI:
10.1007/BF01323482

Publication date:
1989

Z. Phys. B – Condensed Matter 76, 3–15 (1989)

Condensed Matter
Zeitschrift für Physik B

Original contributions

On the theory of layered high-temperature superconductors

T. Schneider, H. De Raedt*, and M. Frick**
IBM Research Division, Zurich Research Laboratory, Rüschlikon, Switzerland

Received March 7, 1989

Assuming that charge carriers form a Fermi liquid state, we study a model for layered high-temperature superconductors with unretarded intralayer and interlayer pairing. Guided by band structure calculations and inverse photoemission experiments, we adopt a tight binding band with nearest and next-nearest neighbors hopping within the sheets and weak interlayer hopping. The gap equations are solved numerically, without imposing a cutoff energy, characteristic to phonon mediated superconductivity. On this basis we calculate the gap parameters, T_c, the tunneling conductance, infrared absorption and the coherence length for various band fillings $\rho = 1/2 - x$ by introducing excess holes of concentration x. Assuming the interlayer coupling strength to be smaller than the intralayer one, our main results are as follows: T_c is dominated by the intralayer properties, reaching a maximum at $x \approx 0.3$, where strong coupling features appear. In the presence of interlayer pairing, the gap becomes anisotropic perpendicular to the layers, and standard BCS-behavior is modified. In particular the BCS-square root singularity in the density of states and in the tunneling conductance is replaced by van Hove singularities characterizing the anisotropic gap. In particular, we investigate the anisotropy of the tunneling conductance for specular and diffuse tunneling for a junction parallel or perpendicular to the layers, infrared absorption, as well as the coherence length, parallel and perpendicular to the layers.

1. Introduction

There is considerable evidence that the $X_m Ca_{n-1} Ba_2 Cu_n O_{2(n+1)+m}$ families (X = Tl, Bi) [1–5] of high-temperature superconductors are highly anisotropic compounds [6–7]. Their properties clearly reveal layered behavior. In fact the zero temperature correlation length, perpendicular to the layers, appears to be smaller than the mean spacing. Consequently, viewing them as anisotropic superconductors is not sufficient. Such a treatment is valid only when the order parameter varies slowly on the scale of the layer separation, which limits the applicability to a small range of temperatures near the transition temperature.

Recently, we presented a model [6–8], treating these compounds as layered superconductors and allowing inequivalent layers and couplings within a unit cell. In the mean-field approximation the interlayer coupling, mediated by a small hopping term, was found to leave T_c unaffected. Thus, a three-dimensional pairing mechanism with high cutoff energy was required to explain the observed dependence of T_c on the average layer spacing. Here we adopt and extend this model. We assume the existence of Fermi liquid states described by a tight binding band resulting from intralayer hopping between nearest and next-nearest neighbors and weak next-nearest neighbor interlayer hopping. Both intra- and interlayer pairing interactions are assumed to be nonretarded and parametrized in terms of coupling constants. Thus the model differs markedly from the standard BCS-picture [9], where a low energy cutoff, originating from the phonon mediated pairing interaction, is introduced. In fact, for pairing interactions with high or no cutoff energy, the entire band is subject to pairing. The presence of interlayer pairing leads to an anisotropic gap. Accordingly, the interpretation

* *Permanent address:* Department of Physics, Universitaire Instelling Antwerpen, NL
** *Permanent address:* Institut für Theoretische Physik, Universität Heidelberg, FRG

of experimental data based on conventional BCS-expressions might not be appropriate.

In this paper we concentrate on systems with one CuO_2 layer per unit cell, such as $Bi_2Ba_2CuO_6$, $Tl_2Ba_2CuO_6$ or $TlBaCuO_5$, adopting a realistic band structure for the valence band. Guided by band structure calculations [10] and photoemission experiments [11–13], we invoke a tight binding band for 0-derived states in the CuO_2-layers, including nearest and next-nearest neighbor hopping within the layers and a small hopping term between adjacent sheets. Starting from a half-filled band, the filling is reduced via excess holes introduced by doping or charge transfer from BiO or TlO layers. The effective pairing interaction is parametrized in terms of the intralayer and interlayer coupling constants g_0 and g_1. We assume $g_0 > |g_1|$ to obtain a nodeless gap. Its anisotropy is then entirely due to the interlayer pairing interaction. Our previous analysis [6–8] of T_c versus interlayer spacing revealed that the pairing is of three-demensional nature and caused by a nonretarded interaction. Thus, in solving the gap equation we do not impose an energy cutoff. This is just the opposite of the phonon-induced interaction, where the excitation energy is small compared to the Fermi energy. On this basis, the gap equation is solved numerically, to obtain estimates for the gap parameters and T_c as a function of band filling. These estimates are then used to calculate the density of states, the tunneling I–V-characteristic, as well as the real part of the conductivity, relevant for infrared absorption, to explore the implications of gap anisotropy, stemming from the interlayer interaction. Here we concentrate on the zero temperature behavior; finite temperature properties will be treated in a forthcoming paper [14].

The anisotropy of the gap and the absence of a low energy cutoff requires that both tunneling current and conductivity must be treated beyond standard BCS and other approximations [9], where the tunneling matrix element is assumed to be constant for states close to the Fermi surface and the current operator in the conductivity is described by the free particle expression. Here we adopt the tight binding expression for the current and consider specular and diffuse tunneling for tunneling current parallel or perpendicular to the layers. Due to the anisotropy of the gap and the absence of a low energy cutoff, new features occur, which should be searched for experimentally in high-quality single crystals. Such experiments should yield important clues on the pairing mechanism and the electronic states involved in superconductivity.

In Sect. 2 we sketch the model, the gap equation and its linearized version used to determine T_c. We also derive the weak coupling solution, the basic expressions for the tunneling current and the real part of the conductivity. In evaluating the tunneling current we consider three model situations: constant tunneling matrix element, specular and diffuse tunneling. In the specular case, the tunneling current is found to depend sensitively on the orientation of the interface with respect to the layers. Moreover, the anisotropy of the gap substantially modifies the standard BCS-behavior of the conductance. At normal incidence infrared absorption can be expressed in terms of the real part of the conductivity. It depends on the polarization of the incoming radiation, as well as on the orientation of this wavevector with respect to the layers. Thus, anisotropic behavior can be expected. Finally we consider the coherence length in the ground state. It is obtained from the correlation function of two quasiparticles whose spins are antiparallel. The anisotropy of the coherence length reflects the ratio of the couplings between and within the layers.

In Sect. 3, we present and discuss our numerical results. For the half-filled band and $g_0 > |g_1|$, T_c is rather insensitive to the specific g_1-value. The zero temperature gap, however, becomes anisotropic perpendicular to the layers for any finite g_1, but remains nodeless. It varies between a minimum and maximum value. Thus the standard BCS-result $2\Delta/k_B T_c \approx 3.52$ no longer applies, although the weak coupling solution of the gap equation represents an excellent approximation. In the presence of interlayer pairing, the density of states differs markedly from the standard BCS-behavior. Due to the anisotropy it becomes nonzero for energies exceeding the minimum value of the gap and exhibits peak features, characterizing the anisotropy. Similarly, the tunneling conductance is heavily affected by the anisotropy of the gap. It differs from zero for voltages exceeding the minimum gap value. Moreover, the assumption of a constant tunneling matrix element is not justified for reasonable values of junction parameters. In fact the conductances in the specular and diffuse limits depend sensitively on the orientation of the junction with respect to the layers. This offers the possibility to clarify the presence of interlayer pairing experimentally. Similarly, for an anisotropic gap, the real part of the conductivity, related to infrared absorption, also differs from the standard BCS-behavior. In fact absorption sets in for frequencies exceeding twice the minimum gap. Thus estimates for $2\Delta_{\min}/k_B T_c$ can be obtained from the onset of absorption. Furthermore infrared absorption strongly depends on the polarization of the incoming light and the orientation of the light wavevector.

We also evaluated T_c as a function of hole concentration x. A maximum is found for $x \approx 0.3$. Moreover,

the weak coupling solution ceases to be adequate with increasing x. Concentrating on $x=0.25$, T_c is not strongly affected by the interlayer pairing interaction unless $g_0 \approx |g_1|$. This also applies to the gap, because the isotropic part dominates. Nevertheless the small anisotropic part affects the density of states and the tunneling conductance, while the influence on the real part of the conductivity, remains small. Accordingly, the effects of the interlayer pairing interaction ($g_0 < |g_1|$) become smaller with increasing hole concentration x. Finally, the coherence length mirrors the strong anisotropy of the ratio between the band widths within and perpendicular to the layers. For $\rho=1/2$ we obtain $\xi_{oz}/\xi_{ox} \approx 0.05\, s/a$, while a smaller anisotropy is obtained for $\rho=1/4$, namely $0.2\, s/a$. a is the lattice constant within the layers and s denotes the layer spacing. These values are within the range of estimates obtained from upper critical field measurements.

In summary, our model seems to include the essential ingredients to describe the superconducting properties of layered high-temperature superconductors. It should be kept in mind, however, that we considered the special case of one layer per unit cell. Summary and conclusions are presented in Sect. 4.

2. Model

We consider the Hamiltonian

$$\mathcal{H} = \mathcal{H}_0 + \mathcal{H}_{\text{int}}, \tag{1}$$

where

$$\mathcal{H}_0 = \sum_{\mathbf{k}_\parallel n\sigma} [\varepsilon(\mathbf{k}_\parallel) c^+_{\mathbf{k}_\parallel n\sigma} c_{\mathbf{k}_\parallel n\sigma} - t(c^+_{\mathbf{k}_\parallel n\sigma} c_{\mathbf{k}_\parallel n+1\sigma} + \text{c.c.})], \tag{2}$$

describes the quasiparticle 0-derived band, including the interlayer hopping of strength t. n labels the layers, $\mathbf{k}_\parallel$ the wavevector within the layers and σ the spin. Guided by recent band structure calculations [10] and angular resolved photoemission experiments [11], we adopt the tight binding band

$$\varepsilon(\mathbf{k}) = A[-2(\cos(k_x a) + \cos(k_y a)) + 4B\cos(k_x a)\cos(k_y a) - 2C\cos(k_z s) - \mu]. \tag{3}$$

a is the lattice constant of the square lattice within the layers and s the spacing between them. $-2A$ represents the nearest neighbor hopping matrix element, $4AB$ the next-nearest neighbor one, and $AC=t$.

There is considerable evidence that superconductivity in the Cu-O based superconductors is correlated with the concentration of O2p-holes in the originally half-filled valence band [11, 12]. Thus, we also consider fillings $\rho = 1/2 - x$, where x corresponds to the concentration of excess holes. Following Ref. 10 we adopt $B=0.45$ and according to the observed dispersion [11], we take $A=0.153$ eV to fix our energy scale. For $\rho=1/2$ the Fermi surface cross section in the x, y-plane is a rounded square, while it is a corrugated cylinder perpendicular to the layers. The corrugation comes from the interlayer hopping term t in (2). For lower filling, the Fermi surface becomes more complicated and open for certain k_z-values.

For fixed filling ρ, $\mu = E_F$ is given by

$$\rho = \frac{1}{N^3} \sum_{\mathbf{k}} (e^{\beta\varepsilon(\mathbf{k})} + 1)^{-1}, \tag{4}$$

N is the number of sites. A fully filled band, where $\rho=1$, corresponds to one quasiparticle of given spin per site. For the pairing interaction we assume

$$\mathcal{H}_{\text{int}} = -\sum_{\substack{\mathbf{k}_\parallel \mathbf{k}'_\parallel \mathbf{k}''_\parallel \\ nm\sigma}} g_{nm} c^+_{\mathbf{k}_\parallel n\sigma} c^+_{-\mathbf{k}_\parallel + \mathbf{k}''_\parallel m-\sigma} \cdot c_{-\mathbf{k}'_\parallel + \mathbf{k}''_\parallel m-\sigma} c_{\mathbf{k}'_\parallel n\sigma}, \tag{5}$$

where

$$g_{nm} = g_0 \delta_{nm} + g_1(\delta_{n,m-1} + \delta_{n,m+1}). \tag{6}$$

g_0 is the strength of the intralayer interaction, while the second term describes the interlayer interaction.

Assuming singlet pairing the gap equation reads [9],

$$\Delta(k_\perp) = \tfrac{1}{2} \sum_{\mathbf{q}} V(q_\perp - k_\perp) \frac{\Delta(q_\perp)}{E(\mathbf{q})} \tanh\left(\frac{\beta E(\mathbf{q})}{2}\right), \tag{7}$$

where

$$V(q_\perp) = g_0 + 2g_1 \cos(q_\perp s), \tag{8}$$

$$E(\mathbf{q}) = (\varepsilon^2(\mathbf{q}) + \Delta^2(q_\perp))^{\frac{1}{2}}, \tag{9}$$

$$\Delta(q_\perp) = \Delta_0 + 2\Delta_1 \cos(q_\perp s). \tag{10}$$

The isotropic term in the gap stems from the constant intralayer interaction g_0, while the anisotropic term is due to the interlayer contribution. Substituting (8) and (10) into (7), we obtain for Δ_0 and Δ_1 the nonlinear equations

$$\begin{aligned} \Delta_0 &= \frac{g_0}{2}(\Delta_0 f_0 + 2\Delta_1 f_1), \\ \Delta_1 &= \frac{g_1}{2}(\Delta_0 f_1 + 2\Delta_1 f_2), \end{aligned} \tag{11}$$

where

$$f_n = \sum_{\mathbf{q}} (\cos(q_\perp s))^n \frac{1}{E(\mathbf{q})} \tanh\left(\frac{\beta E(\mathbf{q})}{2}\right). \tag{12}$$

In solving these equation, we do not impose a low energy cutoff. This differs from the standard BCS-treatment, where the phonon energies are small compared to the Fermi energy. Here we assume pairing caused by a high-energy, non-retarded interaction. At T_c, where the gap vanishes, f_n reduces to

$$\tilde{f}_n = \sum_{\mathbf{q}} (\cos(q_\perp s))^n \frac{1}{\varepsilon(\mathbf{q})} \tanh\left(\frac{\beta_c \varepsilon(\mathbf{q})}{2}\right). \tag{13}$$

T_c is then given by the highest temperature for which

$$\left(1-\frac{g_0}{2}\tilde{f}_0\right)(1-g_1\tilde{f}_2)-\tfrac{1}{2}g_0 g_1 \tilde{f}_1^2 = 0. \tag{14}$$

Because the only dependence on $q_\perp$ comes from the interlayer hopping term with strength t (2), which is small compared to the bandwidth within the layers

$$\frac{2|t|}{W_\parallel} \ll 1, \tag{15}$$

we expect

$$\tilde{f}_1 \approx 0; \quad \tilde{f}_2 \approx \tfrac{1}{2}\tilde{f}_0 \tag{16}$$

to hold. T_c then follows from (14)

$$\left(1-\frac{g_0}{2}f_0\right)\left(1-\frac{g_1}{2}f_0\right) \approx 0. \tag{17}$$

Thus for $g_0 > |g_1|$, T_c is dominated by the intralayer pairing interaction, given by the solution of

$$1 = \frac{g_0}{2} f_0. \tag{18}$$

to a good approximation. Far below T_c and in particular at $T=0$, the full nonlinear equations (11) must be treated, where also the anisotropy of the gap enters. Here the interlayer interaction must be fully taken into account and leads to an anisotropic gap (10).

To derive the weak coupling expression for T_c, we rewrite (18) in the form

$$\begin{aligned} 1 &\approx \frac{g_0}{2}\int_{\varepsilon_B}^{\varepsilon_T} \mathrm{d}x \sum_{\mathbf{k}} \delta(x-\varepsilon(\mathbf{k}))\frac{1}{\varepsilon(\mathbf{k})}\tanh\left(\frac{\beta_c\varepsilon(\mathbf{k})}{2}\right) \\ &= \frac{g_0}{2}\int_{\varepsilon_B}^{\varepsilon_T} \mathrm{d}x\, N_N(x)\frac{1}{x}\tanh\frac{\beta_c x}{2}; \end{aligned} \tag{19}$$

ε_T, ε_B denote the top and bottom of the band and

$$N_N(x) = \sum_{\mathbf{k}} \delta(x-\varepsilon(\mathbf{k})) \tag{20}$$

is the density of states in the normal state. Assuming a slowly varying density of states and $\beta_c\varepsilon_T$, $\beta_c|\varepsilon_B| \gg 1$, the integral yields

$$T_c \approx 1.13\,\theta \exp\left(-\frac{1}{N_N(0)\,g_0}\right), \tag{21}$$

where $$k_B\theta = (\varepsilon_T|\varepsilon_B|)^{1/2}. \tag{22}$$

This is the weak coupling solution of (18), valid for $T_c/\theta \ll 1$. Comparison with the numerical solution of the full nonlinear equation for T_c, will allow the coupling regime and the energy interval $k_B\theta$ where pairing effectively takes place to be determined.

On the basis of the gap parameters Δ_0 and Δ_1 it is now possible to calculate other properties of interest, including their temperature dependence. In these properties we hope to identify features due to the layered nature of the material, i.e. to estimate the parameters characterizing the pairing interaction and the band structure. As noted above, the pairing interaction considered here is not cut off so that the entire band of the Fermi liquid states is allowed to participate in the pairing. In this view, due to the presence of anisotropy, the density of states, the low-temperature tunneling conductance and infrared absorption are expected to deviate substantially from the standard BCS-behavior. Another important issue is how properties change with the band filling.

In the superconducting state the density of states is given by

$$N_S(E) = \sum_{\mathbf{k}} \delta(E - \sqrt{\varepsilon^2(\mathbf{k}) + \Delta^2(k_\perp)}), \tag{23}$$

and vanishes for $E < \Delta_{\min}$.

Next we calculate the tunneling current between a normal metal and such a superconductor, since it is approximately related to the density of states in the superconducting state. According to the transfer Hamiltonian approach [15] valid for weak transmission, the tunnel current at zero temperature is given by [9]

$$\begin{aligned} I = \pm 2\pi e \sum_{\mathbf{kp}} |T_{\mathbf{kp}}|^2 \left(1 \mp \frac{\varepsilon(\mathbf{k})}{E(\mathbf{k})}\right)\theta(|\mathrm{eV}| - E(\mathbf{k})) \\ \cdot\, \delta(\varepsilon_N(\mathbf{p}) - \mathrm{eV} \pm E(\mathbf{k})), \end{aligned} \tag{24}$$

where $\pm$ = sign (eV), $\mathbf{k}$ labels the wavevector on the superconducting side and $\mathbf{p}$ on the normal side. $\varepsilon_N(\mathbf{p})$ describes the conduction band on the N-side, which is assumed to have a constant density of states near the Fermi level. $T_{\mathbf{kp}}$ denotes the tunneling matrix ele-

ment. As a first step, $T_{\mathbf{kp}}$ is assumed to be constant. The tunnel current then reduces to

$$I = \pm 2\pi e |T|^2 N_N(0) \sum_{\mathbf{k}} \left(1 \mp \frac{\varepsilon(\mathbf{k})}{E(\mathbf{k})}\right) \theta(|\mathrm{eV}| - E(\mathbf{k})). \quad (25)$$

$N_N(0)$ is the density of states at the Fermi level on the normal side. This simplification is justified in the standard isotropic BCS-model where due to the low energy cutoff, the variations of the tunneling matrix element $T_{\mathbf{kp}}$ in the relevant $\mathbf{k}$-region remain small. In the usual isotropic case, the $\varepsilon(\mathbf{k})/E(\mathbf{k})$-term cancels. In our model, band structure and gap anisotropy are present. As a result, the tunneling current is expected to differ for a junction parallel or perpendicular to the layers.

We consider two limiting cases, namely specular (coherent) and diffuse (incoherent) tunneling [15]. For specular transmission, where a perfect junction between the normal and superconducting sides is assumed, transverse momenta are conserved. The tunneling matrix element is [15]

$$|T_{\mathbf{kp}}|^2 = P \left|\frac{\partial \varepsilon(\mathbf{k})}{\partial k_L}\right| \cdot \left|\frac{\partial \varepsilon(\mathbf{p})}{\partial p_L}\right| \delta(\mathbf{k}_T - \mathbf{p}_T) D(\varepsilon_L). \quad (26)$$

T and L label transverse and longitudinal components. P denotes a prefactor. The transverse component is parallel to the junction, while the longitudinal one is parallel to the tunnel current. In the WKB approximation D is given by

$$D(\varepsilon_L) = \exp\left[-2 \int_0^d \mathrm{d}x \sqrt{\frac{2m^*}{\hbar}(U(x) - \varepsilon_L)}\right]; \quad (27)$$

d denotes the width and U the height of the junction barrier measured from the Fermi level and ε_L is the energy associated with the motion along x, which is parallel to the tunneling current. Concentrating on effects due to the anisotropic band structure, we assume a constant barrier height $U(x) \equiv U$. We assume the energy ε_L in the junction to be given by the effective mass expression

$$\varepsilon_L = \varepsilon(\mathbf{k}) - \frac{\hbar^2 k_T^2}{2m^*}. \quad (28)$$

Here we used conservation of energy and transverse momentum ($\mathbf{k}_T = \mathbf{p}_T$). Assuming a barrier height which is large compared to $\frac{\hbar^2 k_T^2}{2m^*}$, the square root in (27) can be expanded. The tunneling matrix element becomes approximately

$$|T_{\mathbf{kp}}|^2 = \tilde{C} \left|\frac{\partial \varepsilon(\mathbf{k})}{\partial k_L}\right| \cdot \left|\frac{\partial \varepsilon(\mathbf{p})}{\partial p_L}\right| \delta(\mathbf{k}_T - \mathbf{p}_T) \exp\left(-\frac{k_T^2}{K^2}\right) \quad (29)$$

with

$$K^{-2} = \frac{\hbar d}{\sqrt{2m^* U}}; \qquad \tilde{C} = P \exp\left(-2d\sqrt{\frac{2m^*}{\hbar^2} U}\right). \quad (30)$$

In the estimates presented in Sect. 3, we adopted the following values $d = 10$ Å, $m^* = m_{\mathrm{el}}$ and $U = 1$ eV. To fix k_T we used lattice constants $a = s = 4$ Å. Substitution into (24) yields for the tunneling current in the specular case

$$I = \pm 2\pi e \tilde{C} \sum_{\mathbf{k}} \left|\frac{\partial \varepsilon(\mathbf{k})}{\partial k_L}\right| \cdot \left(1 \mp \frac{\varepsilon(\mathbf{k})}{E(\mathbf{k})}\right) \theta(|\mathrm{eV}| - E(\mathbf{k})) \cdot \exp\left(-\frac{k_T^2}{K^2}\right). \quad (31)$$

Here we neglected the dependence of the tunneling matrix element on the energy difference ε from the Fermi level. It should be kept in mind that L refers to the direction perpendicular to the junction, or parallel to the tunneling current, while T denotes the direction parallel to the junction. Thus the tunneling current is expected to reflect the anisotropy of the gap, of one compares junctions parallel or perpendicular to the layers. Moreover, the differential conductance, i.e. the derivative of the tunneling current with respect to the voltage V, is not simply related to the density of states of the superconductor, because the factor emphasizes small transverse momenta.

As our second limit, we consider diffuse or incoherent tunneling appropriate for junctions with rough interfaces or internal disorder. Here the transverse wavevector components in (26) are no longer correlated. Thus we take [15]

$$|T_{\mathbf{kp}}|^2 = P \left|\frac{\partial \varepsilon(\mathbf{k})}{\partial k_L}\right| \cdot \left|\frac{\partial \varepsilon(\mathbf{p})}{\partial p_L}\right| \cdot \bar{D}, \quad (32)$$

where $\bar{D}$ denotes an average of the D-term (27). In this limit the tunneling current becomes

$$I = \pm 2\pi e N_N(0) P \bar{D} \sum_{\mathbf{k}} \left|\frac{\partial \varepsilon(\mathbf{k})}{\partial k_L}\right| \left(1 \mp \frac{\varepsilon(\mathbf{k})}{E(\mathbf{k})}\right) \cdot \theta(|\mathrm{eV}| - E(\mathbf{k})). \quad (33)$$

In contrast to the specular case (31), the tunneling current will depend less on the orientation of the junction with respect to the layers. Neglecting the gradient

and the ε/E terms, the conductance becomes proportional to the density of states in the superconductor, which reflects gap anisotropy.

Finally we turn to the real part σ_1 of the conductivity, which is related to infrared absorption. This quantity contains information on gap anisotropy. Since σ_1 is related to the current-current-correlation function, we need the tight-binding expression for the current-density operator. Following [9] it is given by

$$\mathbf{j}(\mathbf{R}_n)=(-i)\tfrac{1}{2}\sum_{\delta\sigma} t_\delta \mathbf{R}_\delta [c^+_{n+\delta,\sigma} c_{n\sigma} - c^+_{n\sigma} c_{n+\delta,\sigma}]. \tag{34}$$

n labels sites, δ neighbors with position vectors $\mathbf{R}_\delta$ and t_δ is the corresponding hopping matrix element of the Hamiltonian (2)

$$t_\delta = \langle n|\mathscr{H}|n+\delta\rangle. \tag{35}$$

Fourier transformation yields

$$\mathbf{j}(\mathbf{q})=\sum_{\mathbf{k}\sigma} c^+_{\mathbf{k}+\mathbf{q},\sigma} c_{\mathbf{k}\sigma} \cdot \left[\sum_\delta \mathbf{R}_\delta t_\delta \sin\left(\left(\mathbf{k}+\frac{\mathbf{q}}{2}\right)\mathbf{R}_\delta\right) e^{i\mathbf{q}/2\mathbf{R}_\delta}\right]. \tag{36}$$

According to the adopted band structure (3) we consider nearest neighbors and, within the planes, next-nearest neighbors as well. This leads to

$$\mathbf{j}(\mathbf{q})=\sum_{\mathbf{k}\sigma} c^+_{\mathbf{k}+\mathbf{q},\sigma} c_{\mathbf{k}\sigma} \mathbf{f}(\mathbf{k},\mathbf{q}) \tag{37}$$

with

$$\begin{aligned} f_x(\mathbf{k},\mathbf{q}) = 2aA\Big\{ & -\sin\left(\left(k_x+\frac{q_x}{2}\right)a\right)\cos\left(\frac{q_x}{2}a\right) \\ & +2B\Big[\sin\left(\left(k_x+\frac{q_x}{2}\right)a\right)\cos\left(\left(k_y+\frac{q_y}{2}\right)a\right) \\ & \cdot \cos\left(\frac{q_x}{2}a\right)\cos\left(\frac{q_y}{2}a\right) \\ & -\cos\left(\left(k_x+\frac{q_x}{2}\right)a\right)\sin\left(\left(k_y+\frac{q_y}{2}\right)a\right) \\ & \cdot \sin\left(\frac{q_x}{2}a\right)\sin\left(\frac{q_y}{2}a\right)\Big]\Big\}, \end{aligned}$$

$$\begin{aligned} f_y(\mathbf{k},\mathbf{q}) = 2aA\Big\{ & -\sin\left(\left(k_y+\frac{q_y}{2}\right)a\right)\cos\left(\frac{q_y}{2}a\right) \\ & +2B\Big[\sin\left(\left(k_y+\frac{q_y}{2}\right)a\right)\cos\left(\left(k_x+\frac{q_x}{2}\right)a\right) \\ & \cdot \cos\left(\frac{q_x}{2}a\right)\cos\left(\frac{q_y}{2}a\right) \\ & -\cos\left(\left(k_y+\frac{q_y}{2}\right)a\right)\sin\left(\left(k_x+\frac{q_x}{2}\right)a\right) \\ & \cdot \sin\left(\frac{q_x}{2}a\right)\sin\left(\frac{q_y}{2}a\right)\Big]\Big\}, \end{aligned}$$

$$f_z(\mathbf{k},\mathbf{q}) = 2sA\cdot C\sin\left(\left(k_z+\frac{q_z}{2}\right)s\right)\cos\left(\frac{q_z}{2}s\right).$$

Here we adopted the notation introduced in (3) for the hopping matrix elements. For free electrons (37) reduces to

$$\mathbf{f}_{\text{free}}(\mathbf{k},\mathbf{q})=\mathbf{k}+\frac{\mathbf{q}}{2}.$$

Following [9] the real part of the conductivity tensor then reads

$$\begin{aligned} \sigma_{1\alpha\beta}(\mathbf{q},\omega) = & \frac{2e^2\pi}{m^2\omega}\sum_{\mathbf{p}} f_\alpha(\mathbf{p},\mathbf{q}) f_\beta(\mathbf{p},\mathbf{q}) \\ & \cdot \delta(\omega - E(\mathbf{p}) - E(\mathbf{p}+\mathbf{q})) \\ & \times (v^2_{\mathbf{p}} u^2_{\mathbf{p}+\mathbf{q}} - u_{\mathbf{p}} v_{\mathbf{p}} u_{\mathbf{p}+\mathbf{q}} v_{\mathbf{p}+\mathbf{q}}), \end{aligned} \tag{38}$$

where

$$v^2_{\mathbf{p}} = \frac{1}{2}\left(1-\frac{\varepsilon(\mathbf{p})}{E(\mathbf{p})}\right); \quad u^2_{\mathbf{p}} = \frac{1}{2}\left(1+\frac{\varepsilon(\mathbf{p})}{E(\mathbf{p})}\right). \tag{39}$$

Absorption requires $\sigma_{1\alpha\beta}(\mathbf{q},\omega)\neq 0$ and involves the creation of pairs of quasiparticles at a minimum frequency of $2\Delta_{\min}$. Due to the tensorial nature of $\sigma_{1\alpha\beta}$ and its $\mathbf{q}$-dependence, absorption depends on light polarization and reflects gap and band structure anisotropy. In infrared absorption, although the experiment is done at one particular frequency, the wavevectors involved are determined by the boundary conditions and the parameters of the superconductor. The simplest case is where the coherence length is much less than the penetration depth and $\omega<2\Delta_{\min}$. Here $\sigma_{1\alpha\beta}$ vanishes for all $\mathbf{q}$. Therefore there is no absorption and light is perfectly reflected. For $\omega>\Delta_{\min}$, absorption occurs, and the magnitude of the relevant wavevectors is smaller than the inverse penetration depth.

The coherence length in the ground state can be obtained by considering the correlation function of two quasiparticles at position $\mathbf{r}_1$ and $\mathbf{r}_2$, whose spins are antiparallel. It is given by [16]

$$\mathbf{F}(\mathbf{r}_1-\mathbf{r}_2)=F(\mathbf{r})=\sum_{\mathbf{k}} u_{\mathbf{k}} v_{\mathbf{k}} e^{-i\mathbf{k}\cdot\mathbf{r}} = \frac{1}{2}\sum_{\mathbf{k}} \frac{\Delta(k_\perp)}{E(\mathbf{k})} e^{-i\mathbf{k}\cdot\mathbf{r}}. \tag{40}$$

For a spherical Fermi surface and an isotropic gap, $F(\mathbf{r})$ decays exponentially $\sim\exp-(r/\xi_0)$ for $r<\xi_0$

where $\xi_0 = \frac{\hbar^2 k_F}{m\Delta}$. In the anisotropic case, we set $r = (x, y, z)$ and estimate ξ_{ox} and ξ_{oz} from the exponential decay of the correlation function along x or z. Due to the assumption of weak interlayer hopping (15), the ratio ξ_{oz}/ξ_{ox} will be small.

3. Numerical results

Half-filled band

To explore the influence of the interlayer coupling on the gap and T_c, we first consider the half-filled band. The value $g_0 = 1$, together with $g_1 = 0$, was chosen because these values yield a rather low T_c, namely $k_B T_c = 0.013\,A$, corresponding to $T_c = 23$ K. $A = 0.153$ eV being the energy unit, introduced in (3). T_c can be raised by reducing the band filling $\rho = 1/2 - x$ via excess holes of concentration x. The estimates listed in Table 1 reveal, in agreement with (17)–(19), that unless for $g_0 \approx |g_1|$, the interlayer pairing does not affect T_c very much, while the gap parameters and in turn the minimum and maximum values of the gap vary markedly. Thus, the conventional BCS-expression for an isotropic gap is no longer applicable. Even though the interlayer coupling does not affect T_c much, it is of course needed, together with the interlayer hopping, to establish 3-dimensional superconductivity. From Table 1 it is also seen that for g_1 approaching g_0 the interlayer pairing substantially increases T_c.

To identify the weak coupling regime we also calculated the gap for $g_1 = 0$ for several g_0 values. The results are summarized in Table 2 and Fig. 1 shows the plot of $\ln(k_B T_c)$ versus $1/(N_N(0)\,g_0)$, revealing the presence of weak coupling (23), with a cutoff energy $k_B\theta \approx 3.28$ ($\hat{=} 5821$ K), which is comparable to the band width (1.16 eV) (Fig. 2) and thus large compared to $k_B T_c$.

Table 1. Numerical estimates for Δ_0, Δ_1 and T_c as obtained from (11) and (14) for $\rho = 1/2$, $B = 0.45$, $C = 0.1$ (3). Energies are in units of 0.153 eV, $\Delta_{\min}$ denotes the minimum and $\Delta_{\max}$ the maximum value of the gap

g_0	g_1	Δ_0	Δ_1	$k_B T_c$	$\frac{2\Delta_{\min}}{k_B T_c}$	$\frac{2\Delta_{\max}}{k_B T_c}$
1	−0.99	0.0232	0.00067	0.0131	3.34	3.75
1	−0.9	0.0232	0.00063	0.0131	3.35	3.73
1	−0.8	0.0232	0.00059	0.0131	3.36	3.72
1	−0.6	0.0233	0.00049	0.0132	3.38	3.68
1	−0.4	0.0233	0.00036	0.0132	3.42	3.64
1	−0.2	0.0235	0.00020	0.0132	3.50	3.62
1	0	0.0235	0	0.0133	3.53	3.53
1	0.2	0.0236	−0.0003	0.0134	3.43	3.61
1	0.4	0.0237	−0.0006	0.0135	3.33	3.69
1	0.6	0.0239	−0.0013	0.0138	3.09	3.84
1	0.8	0.0243	−0.0026	0.0146	2.62	4.04
1	0.9	0.0244	−0.0039	0.0158	2.10	4.08
1	0.99	0.0244	−0.0061	0.0186	1.32	3.92

Table 2. Numerical estimates for Δ_0 and T_c for $g_1 = 0$, $B = 0.45$, $C = 0.1$, as obtained from (11) and (14). $N_N(0) = 0.18$ is the density of states in the normal state at the Fermi energy $E_F = -0.891$. Energies are in units of 0.153 eV

g_0	Δ_0	$k_B T_c$	$\frac{2\Delta_0}{k_B T_c}$	$\frac{1}{N_N(0)\,g_0}$
0.6	0.00051	0.00028	3.64	9.26
0.8	0.0058	0.00330	3.52	6.94
1.0	0.02380	0.01340	3.55	5.56
1.2	0.06080	0.03440	3.53	4.63
1.4	0.11900	0.06720	3.54	3.97
1.5	0.15500	0.08760	3.54	3.70
2.0	0.38400	0.21100	3.64	2.78

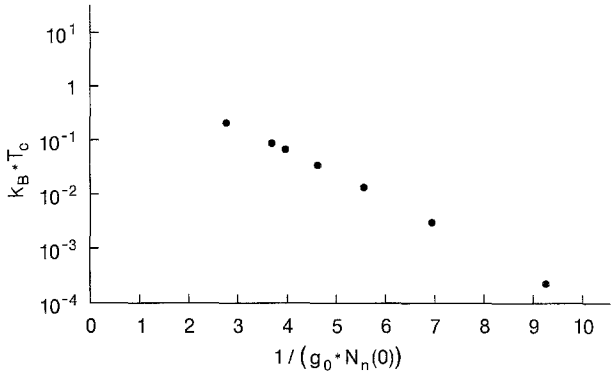

Fig. 1. $\ln k_B T_c$ versus $1/(N_N(0)\,g_0)$ for the data listed in Table 2

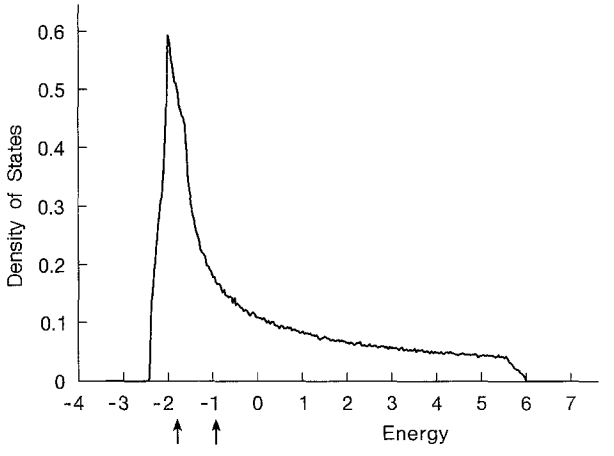

Fig. 2. Density of states $N_N(E)$ of the normal state for the band given by (3) with $B = 0.45$, $t = 0.1$. The arrows mark the Fermi energies for $\rho = \frac{1}{2}$ ($E_F = -0.891$) and $\rho = \frac{1}{4}$ ($E_F = -1.76$)

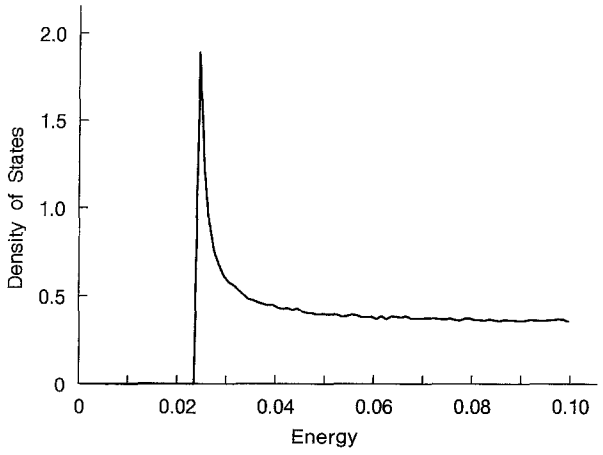

Fig. 3. Density of states $N_s(E)$ of the superconducting state for $\Delta_0 = 0.0244$ and $\Delta_1 = 0$, corresponding to the standard BCS-case. Energies are in units of 0.153 eV

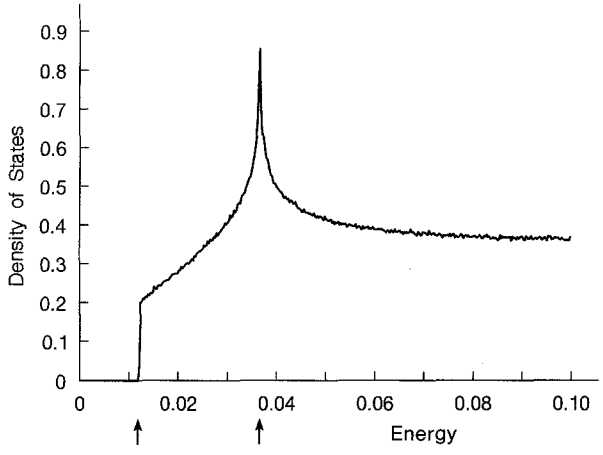

Fig. 4. $N_s(E)$ for $\Delta_0 = 0.0244$ and $\Delta_1 = -0.006$, corresponding to the solution of (11) and (14) for $\rho = 1/2$, $g_0 = 1$, $g_1 = 0.99$ as listed in Table 1. The arrows mark the minimum ($\Delta_{min} = 0.0124$) and the maximum ($\Delta_{max} = 0.0364$) of the gap. Energies are in units of 0.153 eV

In Figs. 3 and 4 we depicted the density of states in the superconducting state to illustrate and contrast the cases of an isotropic and anisotropic gap. The isotropic case corresponds to the standard BCS-behavior with a square root singularity at $E = \Delta_0$. In the anisotropic case (Fig. 4), the square root singularity is removed and $N_S(E)$ differs from zero for energies exceeding the minimum of the gap. Due to the interlayer pairing interaction, the gap anisotropy perpendicular to the layers is seen to affect the density of states between Δ_{min} and Δ_{max}. In particular, a pronounced peak appears at Δ_{max}, corresponding to a Van Hove singularity.

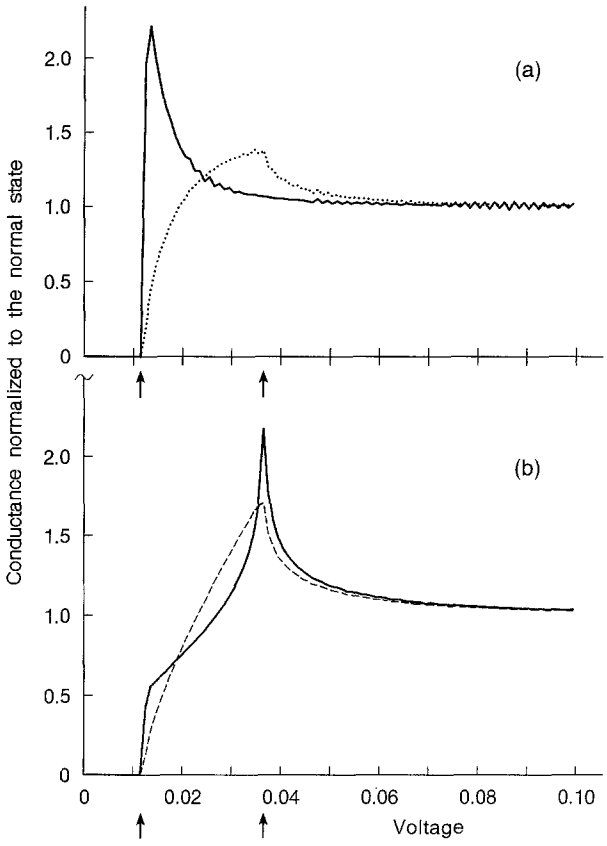

Fig. 5a and b. Tunneling conductance versus voltage for anisotropic tunneling according to (31) for specular and (33) for diffuse tunneling for $\Delta_0 = 0.0244$; $\Delta_1 = -0.0061$. The other parameters are identical to those in Fig. 4. Solid line: tunneling parallel to the layers; dashed line: tunneling perpendicular to the layers. **a** Specular tunneling, **b** diffuse tunneling. The arrows mark Δ_{min} and Δ_{max}

This behavior affects the tunneling current and the tunneling conductance. Assuming a constant tunneling matrix element, the conductance is closely related to the density of states (25), apart from a slight asymmetry between positive and negative voltages, coming from the ε/E-term. Because this term turns out to be small, the tunneling conductance becomes indeed nearly proportional to the density of states shown in Figs. 3 and 4, provided the assumption of a constant tunneling matrix element is justified. In any case, the removal of the standard BCS-square root singularity by the gap anisotropy (Fig. 4) indicates that the evaluation of the gap parameters from measured data will be nontrivial, even for excellent samples and junctions.

If we take anisotropy into account and make more realistic assumptions about the tunneling matrix element, the conductance depends sensitively on the orientation of the junction with respect to the crystal. Figure 5 depicts the conductance in the super-

conducting state normalized to that in the normal state values at zero temperature. Especially in the specular case (Fig. 5a) we see striking differences between tunneling parallel and perpendicular to the layers. They mainly stem from the exponential term in (31) favoring small wavevectors k_T parallel to the junction or perpendicular to the tunneling current. Thus, for tunneling parallel to the layers, small wavevectors perpendicular to the layers are preferred. As depicted in Fig. 5a, the energy range just above the minimum value of the gap is then favored. For tunneling perpendicular to the layers, all k_z-values contribute, due to the small dispersion in the z-direction. Thus the full gap dispersion is probed, leading to a peak around the maximum value of the gap (cf. also Fig. 4).

For diffuse tunneling (Fig. 5b) we see no striking differences in the normalized conductance for the two tunneling directions. Differences mainly come from the gradient term in (33). This causes no drastic variation of the normalized quantity, even though the absolute values differ substantially due to the different dispersion parallel and perpendicular to the layers. The tunneling conductance nevertheless reflects the minimum and maximum gap.

Due to difficulties in preparing perfect interfaces and defect-free junctions, it appears that diffuse tunneling is closer to the current experimental situation [17, 18]. Thus, it is gratifying that diffuse tunneling reflects the gap anisotropy. Even if smearing of edges and peaks by finite temperature and depairing effects occur, it is clear that standard methods of determining the gap [15] must be reconsidered.

Next we turn to the real part of the conductivity tensor (38), relevant to describe infrared absorption. For $\omega > 2\Delta_{\min}$, where absorption occurs, the relevant wavevectors are smaller than the inverse penetration depth, which is small compared to the inverse coherence length characteristic for the discussed superconductor.

In evaluating $\sigma_{1\alpha\beta}(\mathbf{q}, \omega)$ (38), the Brillouin zone was covered by a grid of $256 \times 256 \times 256$. Thus the smallest meaningful wavevector $\mathbf{q}$ has a magnitude of $\pi/128a$ or $\pi/128s$, which is of the order of the inverse penetration depth. Even for these small wavevectors, $\sigma_{1\alpha\beta}(\mathbf{q}, \omega)$ exhibits a complicated $\mathbf{q}$-dependence so that the evaluation of the reflectivity even for normal incidence becomes complicated. For this reason we consider $\sigma_{1\alpha\beta}(\mathbf{q}, \omega)$ only. Figure 6a shows the frequency dependence of σ_{1yy} and σ_{1zz} for $\mathbf{q} = (\pi/128a, 0, 0)$ parallel to the layers, while σ_{1xx} for $\mathbf{q} = 0, 0, \pi/128s)$ perpendicular to the layers is depicted in Fig. 6b. These elements of the conductivity tensor are relevant for infrared absorption. Moreover, we included the isotropic gap case for comparison.

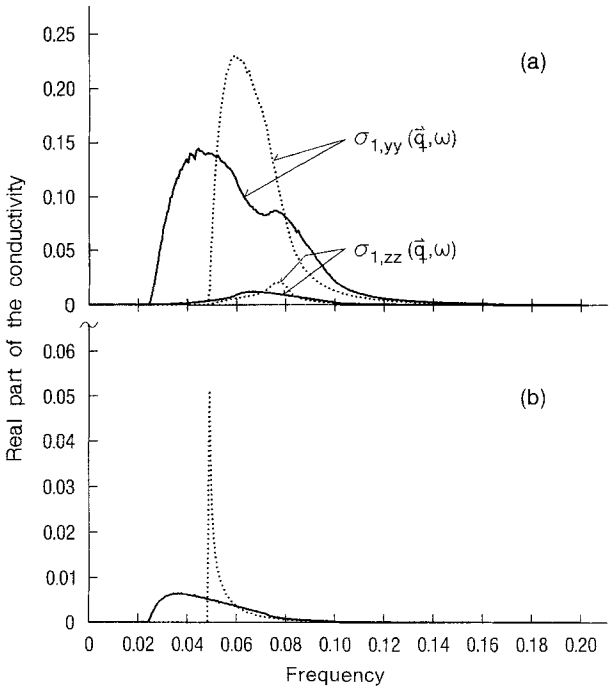

Fig. 6a and b. Real part of the conductivity $\sigma_{1\alpha\alpha}(\mathbf{q}, \omega)$ (38) versus photon energy for $\rho = \frac{1}{2}$, $\Delta_0 = 0.0244$, $\Delta_1 = -0.0061$ (solid line) and $\Delta_1 = 0$ (dashed line). **a** $\mathbf{q} = (q_x, 0, 0)$ parallel to the layers. **b** $\mathbf{q} = (0, 0, q_z)$ perpendicular to the layers

Most importantly, absorption is seen to set in for $\omega > 2\Delta_{\min}$ and there is a significant difference between the two orientations of $\mathbf{q}$. This anisotropy stems from the small bandwidth ratio $W_\perp/W_\parallel$. Thus $\sigma_{1xx}(q_z, \omega)$ (Fig. 6b) exhibits BCS-type behavior in the isotropic case, similar to the density of states. These peaks are removed by gap anisotropy. In any case, infrared measurements yield information for $\Delta_{\min}$ only.

Recently, removal of BCS-behavior, as depicted in Fig. 6b, has been observed in the far infrared conductivity, derived from the reflectivity of an epitaxial $YBa_2Cu_3O_7$ thin film for radiation with the electric field parallel to the a, b-plane [19]. This experimental setup corresponds in our notation to $\mathbf{q} \| z$, where an anisotropic gap leads to a peak structure as depicted in Fig. 6b and observed experimentally. Thus this experiment [19] provides considerable evidence for an anisotropic gap originating from the interlayer pairing interaction.

Finally we turn to the coherence length, as determined from (40). The results listed in Table 3 reflect the strong anisotropy of the bandwidth ratio $W_\perp/W_\parallel$. In particular, ξ_{oz} is found to be smaller than the separation of the layers and the ratio ξ_{oz}/ξ_{ox} is within the range of values estimated from the upper critical fields in the high-temperature superconductors.

Table 3. Numerical estimates of the coherence length ξ_{ox} and ξ_{oz} according to (41) for the parameters cited and the tight binding band given by (3) with $C=0.1$

g	g_0	g_1	Δ_0	Δ_1	ξ_{ox}/a	ξ_{oz}/s	$\frac{\xi_{oz}}{\xi_{ox}}\frac{a}{s}$
1/2	1	0	0.0244	0	7.6	0.39	0.05
1/2	1	0.99	0.0244	−0.0061	7.9	0.47	0.06
1/4	1	0	0.16	0	5.2	0.93	0.2
1/4	1	0.8	0.155	−0.005	5.1	1.07	0.2

Table 4. Numerical estimates for Δ_0 and k_BT_c for various band fillings and $B=0.45$, $C=0.1$ for $g_0=1$ and $g_1=0$ as obtained from (11) and (14). Energies are in units of 0.153 eV

ρ	E_F	$N_N(0)$	Δ_0	k_BT_c	$\frac{2\Delta_0}{k_BT_c}$	$\frac{1}{N_N(0)g_0}$
0.1	−2.03	0.48	0.130	0.068	3.8	2.08
0.15	−1.94	0.58	0.150	0.080	3.69	1.72
0.2	−1.85	0.52	0.160	0.086	3.65	1.92
0.25	−1.76	0.50	0.160	0.085	3.64	2
0.3	−1.65	0.46	0.145	0.080	3.64	2.17
0.35	−1.53	0.34	0.123	0.068	3.61	2.94
0.4	−1.36	0.26	0.085	0.048	3.55	3.85
0.45	−1.15	0.22	0.048	0.027	3.53	4.55
0.5	−0.891	0.17	0.024	0.013	3.53	5.88

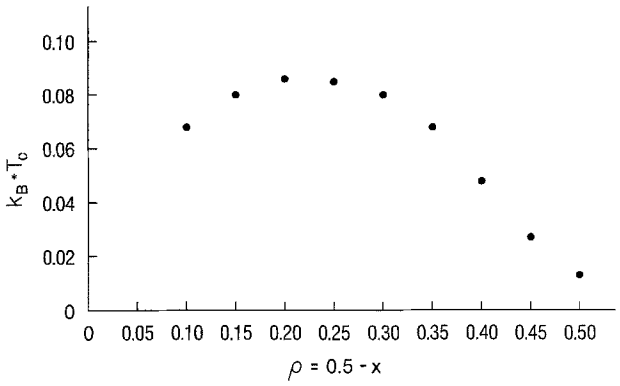

Fig. 7. T_c versus band filling $\rho=1/2-x$ for $B=0.45$, $C=0.1$, $g_0=1$, $g_1=0$. x denotes the concentration of excess holes. Energies are given in units of 0.153 eV

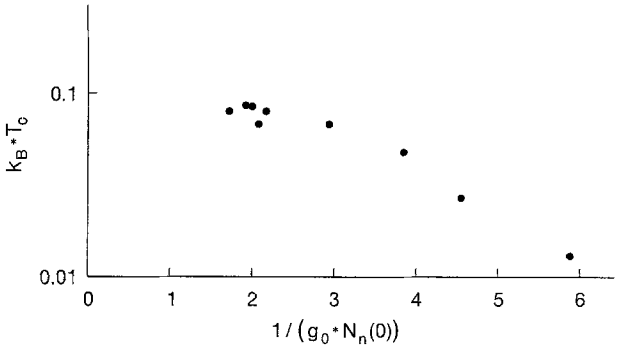

Fig. 8. ln (k_BT_c) versus $1/(N_N(0)g_0)$ for the data listed in Table 3

Reduced band filling

Up to now we have considered only the half-filled band, where $\rho=1/2$. Next we reduce the filling by introducing excess holes of concentration x, so that $\rho=1/2-x$. Thus, the Fermi energy (4) and in turn the superconducting properties will change. To explore this variation, we solved (11) and (14) numerically to estimate the gap Δ_0 and T_c for various fillings ρ. The results are summarized in Table 4, together with other quantities of interest. It is clearly seen that both Δ_0 and T_c first increases as the filling is reduced, reaches a maximum value around $\rho\approx 0.2$ and then decrease for smaller fillings. This x-dependence of T_c is more clearly depicted in Fig. 7. Because the intralayer pairing interaction has been kept fixed, and the density of states (Fig. 2) is seen to follow the same behavior, the variation of Δ_0 and T_c with x must be attributed to variation of the density of states close to the Fermi energy. From Table 4 it is also seen that the density of states can become so large that strong coupling sets in. In fact, the assumption of weak coupling would lead according to Fig. 8 to a cutoff energy $k_B\theta=0.286$, which is only about twice k_BT_c. The appearance of strong coupling is also signaled by the ratio $2\Delta_0/k_BT_c$ which is seen to increase as the filling is reduced.

To explore the influence of the interplanar pairing interaction for $\rho=1/4$, we also varied g_1 from -0.99 to 0.99. The results are summarized in Table 5. In agreement with (18) and in analogy to the half-filled case (Table 1), T_c is practically independent of g_0 for $g_1<|g_0|$. The gap anisotropy, however, increases with g_1 and turns out to be larger for $g_1>0$.

To clarify the implications of strong coupling, we consider the $\rho=1/4$ case in more detail. From the density of states shown in Fig. 2 it is seen that the Fermi energy lies very close to the singularity in the density of states. Thus, the assumption of a constant density of states near the Fermi energy fails and band structure effects are expected. For this purpose we consider $g_0=1$, $g_1=0$ for the isotropic and $g_0=1$, $g_1=0.8$ for the anisotropic case. Figure 9a depicts the density of states for the isotropic case. The standard

Table 5. Numerical estimates for Δ_0, Δ_1, and k_BT_c for $\rho=1/4$ and $B=0.45$, $C=0.1$ for $g_0=1$ and various g_1 values as obtained from (11) and (14). Energies are in units of 0.153 eV

g_1	Δ_0	Δ_1	k_BT_c	$\frac{2\Delta_{min}}{k_BT_c}$	$\frac{2\Delta_{max}}{k_BT_c}$
−0.99	0.155	0.0023	0.0852	3.54	3.75
−0.9	0.155	0.0022	0.0852	3.55	3.75
−0.8	0.155	0.0019	0.0852	3.55	3.74
−0.6	0.155	0.0016	0.0852	3.57	3.72
−0.4	0.155	0.0011	0.0852	3.59	3.69
−0.2	0.155	0.0006	0.0852	3.61	3.67
0.0	0.155	0.0000	0.0852	3.64	3.64
0.2	0.155	−0.0008	0.0853	3.6	3.68
0.4	0.155	−0.0018	0.0853	3.55	3.72
0.6	0.155	−0.0031	0.0855	3.47	3.77
0.8	0.155	−0.0050	0.0855	3.37	3.84
0.9	0.154	−0.0063	0.0864	3.28	3.86
0.99	0.154	−0.0076	0.0764	3.64	4.43

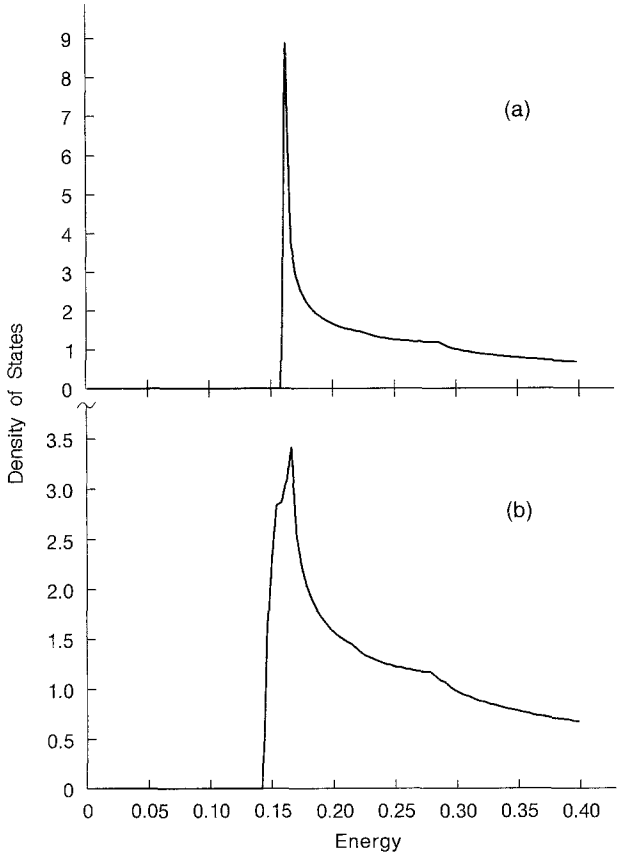

Fig. 9. Density of states $N_s(E)$ for $\rho=1/4$. **a** $g_0=1$, $g_1=0$, $\Delta_0=0.16$, $\Delta_1=0$; **b** $g_0=1$, $g_1=0.8$, $\Delta_0=0.155$, $\Delta_1=-0.005$

BCS-singularity is seen around the gap, while at higher energies band structure features appear. Figure 9b shows the density of states in the anisotropic case, the BCS-singularity is removed and new peak features appear between the minimum and maximum value

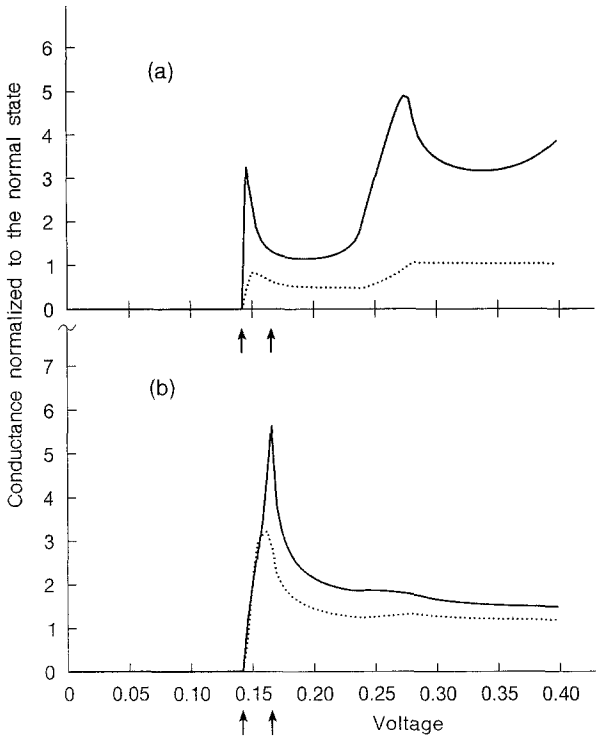

Fig. 10a and b. Tunneling conductance versus voltage for specular (31) and diffuse (33) tunneling for $\Delta_0=0.155$ and $\Delta_1=-0.005$. The other parameters are listed in Table 5. **a** Specular and **b** diffuse transmission. Solid line: tunneling parallel to the layers; dashed line: tunneling perpendicular to the layers. The arrows mark Δ_{min} and Δ_{max}

of the gap. In contrast to the half-filled case, however, the gap anisotropy becomes manifest in a rather narrow energy interval because Δ_1 turns out to be much smaller. In fact, Δ_0 increases markedly with the concentration of excess holes (Table 4), while Δ_1 remains a small correction.

In this view it is not surprising that the effects of an anisotropic gap on the conductance of specular and diffuse tunneling, shown in Fig. 10, are restricted to a rather small voltage interval. Nevertheless, the BCS-singularity is removed. Moreover, specular tunneling is seen to be more sensitive to details in the band structure, as revealed by the second peak in Fig. 10a, reflecting the singularity in the density of states.

Similarly, due to the small anisotropy, the real part of the conductivity (38) is not expected to exhibit pronounced anisotropy effects. In fact, comparison of Figs. 11a and b clearly shows that for frequencies just above $2\Delta_{min}$, the conductivity grows less abruptly in the anisotropic case, because the BCS-type behavior is removed.

Finally we turn to the estimates of the coherence length, evaluated with the aid of (40). From the results

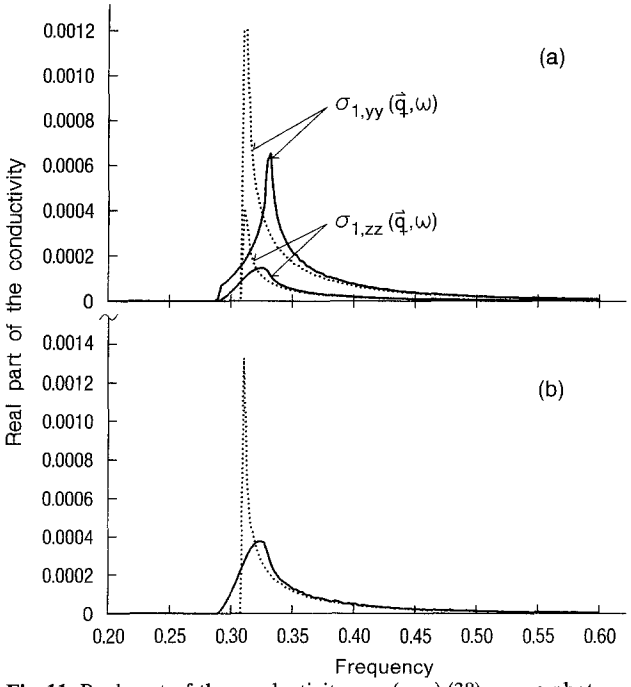

Fig. 11. Real part of the conductivity $\sigma_{1\alpha\alpha}(\mathbf{q}, \omega)$ (38) versus photon energy for $\rho = 1/4$, $\Delta_0 = 0.155$, $\Delta_1 = -0.005$ (solid lines) and $\Delta_1 = 0$ (dashed line). **a** $\mathbf{q} = (q_x, 0, 0)$ parallel to the layers, **b** $\mathbf{q} = (0, 0, q_z)$ perpendicular to the layers

listed in Table 3 it is apparent that excess holes lead to a considerable reduction of the anisotropy. Nevertheless, both ξ_{ox}/a and ξ_{oz}/s are still rather small and ξ_{oz} just reaches the spacing s between the layers.

4. Summary and conclusions

We investigated a model for layered high-temperature superconductors. The model assumes that the mobile charge carriers form a Fermi liquid, moving in a highly anisotropic tight binding band, parametrized in terms of intralayer hopping between nearest and next-nearest neighbors and weak nearest neighbor interlayer hopping. The intra- and interlayer pairing interaction was assumed to be nonretarded and was parametrized in terms of the coupling constants g_0 and g_1 (6). Excess holes of concentration x could also be introduced to reduce the band filling $\rho = 1/2 - x$.

To estimate ground state properties and T_c, we solved the matrix gap equation numerically for singlet pairing and realistic parameters for the highly anisotropic valence band, with bandwidth ratio $W_\perp/W_\parallel = 0.03$. Assuming a nonretarded pairing interaction no energy cutoff was introduced. For $0.1 < \rho < 1/2$, T_c turned out to be rather unaffected by the interlayer pairing interaction unless $g_1 \approx |g_0|$. In this regime the gap turned out to be increasingly anisotropic perpendicular to the layers as $|g_1|/g_0$ is increased, but remains nodeless. To obtain realistic T_c values g_0 was fixed to $g_0 = A = 0.153$ eV. By reducing the band filling $\rho = 1/2 - x$ in terms of excess holes with concentration x, T_c was found to increase, reaching a maximum around $x \approx 0.3$. This behavior was traced back to changes in the density of states (Table 4) at the Fermi energy and the appearance of strong coupling. The ratio of the coherence length ξ_{oz}/ξ_{ox} (Table 3) was found to be consistent with the estimates for real systems, obtained from upper critical field measurements. Thus the model appears to include the essential features to describe the superconducting properties of the $X_m Ca_{n-1} Ba_2 CuO_{2(n+1)+m}$ families. We also studied the tunneling conductance for specular and diffuse transmission, as well as the real part of the conductivity. Our results reveal that tunneling and infrared absorption experiments on homogeneous single crystals should allow an anisotropic gap perpendicular to the layers to be characterized. In fact, gap anisotropy and the lack of a low energy cutoff invalidate standard BCS-behavior and give rise to novel features.

We are grateful to H. Horner, K.A. Müller and K.F. Renk for stimulating discussions and to A. Baratoff for pertinent suggestions and careful reading of the manuscript. M.F. thanks IBM for hospitality and support. H.d.R. would like to thank the National Science Foundation for financial support.

References

1. Michel, C., Hervieu, M., Borel, M.M., Grandin, A., Deslandes, F., Provost, J., Raveau, B.: Z. Phys. B – Condensed Matter **68**, 421 (1987)
2. Hazen, R.M., Finger, L.W., Angel, R.J., Prewitt, C.T., Ross, N.L., Hadidiacos, C.G., Heaney, P.J., Veblen, D.R., Sheng, Z.Z., El Ali, A., Hermann, A.M.: Phys. Rev. Lett. **60**, 1657 (1988)
3. Kondoh, S., Ando, Y., Onoda, M., Sato, M., Akimitsu, J.: Solid State Commun. **65**, 1329 (1988)
4. Zandbergen, H.V., Huang, Y.K., Menken, M.J.V., Li, J.N., Kadovaki, K., Menovsky, A.A., Van Tendeloo, G., Amelinckx, S.: Nature **332**, 620 (1988)
5. Ihara, H., Sugise, R., Hirabayashi, M., Terada, N., Jo, M., Hayashi, K., Negishi, A., Tokumoto, M., Kimura, Y., Shimomura, T.: Nature **334**, 510 (1988)
6. Schneider, T., Baeriswyl, D.: Z. Phys. B – Condensed Matter **73**, 5 (1988)
7. Baeriswyl, D., Schneider, T.: In: Proceedings of the "Mini-Workshop Mechanisms of High Temperature Superconductivity," Trieste, Italy, June 20–July 29, 1988
8. Schneider, T.: IBM Res. Dev.
9. Mahan, G.D.: Many-particle phsysics. New York: Plenum Press 1981
10. Ju, J., Massida, S., Freeman, A.J.: Physica C **152**, 273 (1988)
11. Takahashi, T., Matsuyama, H., Katayama-Yoshida, H., Okabe, Y., Hosoya, S., Seki, K., Fujimoto, H., Sato, M., Inokuchi, H.: Nature **334**, 691 (1988)
12. Himpsel, F.J., Chandrashekhar, G.V., McLean, A.B., Shafer, M.W.: Phys. Rev. B**38** (1988)

13. Imer, J.M., Patthey, F., Dardel, B., Schneider, W.D., Baer, Y., Petroff, Y., Zettl, A.: Phys. Rev. Lett **62**, 336 (1989)
14. Frick, M., Schneider, T., De Raedt, H.: (unpublished)
15. Duke, C.B.: Tunneling in solids, solid state physics. Suppl. 10. New York, London: Academic Press 1969
16. Rickayzen, G.: Theory of superconductivity. New York: Interscience Publishers 1965
17. Viera, S., Ramos, M.A., Vallet-Regi, M., Gonzales-Calbet, J.M.: Phys. Rev. B**38**, 9295 (1988)
18. Shiping, Z., Hongjl, T., Yinfel, Ch., Yifen, Y., Qiansheng, Y.: Solid State Commun. **67**, 1179 (1988)
19. Schutzmann, J., Ose, W., Keller, J., Renk, K.F., Roas, B., Schultz, L., Saemann-Ischenko, G.: (unpublished)

T. Schneider
IBM Research Division
Zurich Research Laboratory
Säumerstrasse 4
CH-8803 Rüschlikon
Switzerland

H. De Raedt
Department of Physics
Universitaire Instelling Antwerpen
Universiteitsplein 1
B-2610 Wilrijk
Belgium

M. Frick
Institut für Theoretische Physik
Universität Heidelberg
Philosophenweg 19
D-6900 Heidelberg 1
Federal Republic of Germany